

# Bio-based Superhydrophobic Sensor for Enhanced Anti-Fouling and Rapid Bacterial Detection in Hematology

Lifen LAN<sup>1</sup>, Xiaoxiao LU<sup>2\*</sup>

<sup>1</sup> Department of Hematology, Affiliated Hospital of Inner Mongolia Medical University, Hohhot City, 010050, Inner Mongolia Autonomous Region, China

<sup>2</sup> Hepatobiliary and Pancreatic Cancer Center, Chongqing University Cancer Hospital, Chongqing, 400030, China

<http://doi.org/10.5755/j02.ms.40980>

Received 25 March 2025; accepted 23 April 2025

Hematology patients are at high risk of nosocomial infections, necessitating rapid and reliable bacterial detection. Current methods, such as culture and polymerase chain reaction (PCR), are often slow, expensive, or susceptible to contamination. This research introduces a novel bio-based superhydrophobic sensor to address these limitations. The sensor utilizes a polydimethylsiloxane (PDMS) and TiO<sub>2</sub> coated substrate to create a superhydrophobic surface (water contact angle >150°), which significantly reduces bacterial adhesion. Detection relies on peptides that undergo a conformational change upon binding specific bacteria, releasing attached magnetic beads. These beads are detected electrochemically using an indium tin oxide (ITO) electrode modified with cadmium telluride (CdTe) quantum dots and graphene oxide (GO) composite, enhancing electron transfer efficiency by 2.3-fold compared with bare ITO. This design achieved rapid (<90 minutes) and sensitive detection. The sensor had high accuracy comparable to PCR and discriminated between *Klebsiella pneumoniae* (*K. pneumoniae*) and *Pseudomonas aeruginosa* (*P. aeruginosa*). By combining anti-fouling properties with specific bacterial recognition and enhanced electrochemical detection, this sensor offers a promising platform for reducing infection risks in hematology.

**Keywords:** bio-based, superhydrophobic, hematology, anti-fouling, bacterial detection, electrochemical sensor, peptide, quantum dots.

## 1. INTRODUCTION

Hematology patients, often undergoing immunosuppressive therapy and experiencing agranulocytosis, face significantly elevated hospital-acquired infections (HAIs) [1]. The World Health Organization reports HAI incidence rates as high as 35 %–50 % in patients with hematological malignancies, with bloodstream infections accounting for 28 % and associated mortality rates of 15 %–30 % [2]. These infections prolong hospital stays (by 40 %–60 %) and increase medical costs substantially [3]. Traditional microbiological culture methods, while the gold standard, require 24–72 hours for results, delaying appropriate treatment [4]. Molecular diagnostic techniques, such as polymerase chain reaction (PCR), are faster (4–8 hours) but are expensive and require specialized equipment and trained personnel [5]. In addition, invasive procedures such as blood transfusions and bone marrow punctures are particularly susceptible to contamination, mainly due to interference from blood components on existing sensors. Existing impedance electrochemical sensors and fluorescence optical sensors are susceptible to non-specific adsorption of fibrinogen and light scattering effects of albumin in blood testing, resulting in a false positive rate 18 %–25 % [6]. Blood disease patients often have compromised immune systems. Among them, blood diseases such as leukemia and lymphoma can disrupt the hematopoietic system function, thereby suppressing the immune system.

The weakened immune system makes patients more susceptible to attacks from viruses and bacteria, leading to infections. In addition, after receiving chemotherapy, bone marrow transplantation, or immunosuppressive therapy, the immune function of leukemia and lymphoma patients will further decline, and the number of immune cells such as neutrophils will decrease, which further increases infection.

Superhydrophobic materials, with their extreme water repellency, offer a promising approach to combat bio-fouling. These materials, characterized by water contact angles exceeding 150° and low sliding angles, minimize the contact area between a liquid (such as blood) and the surface, reducing the adhesion of proteins and cells [7, 8]. This "self-cleaning" effect is primarily due to the hierarchical micro/nanostructure of the surface, which traps air and minimizes the solid-liquid interface [9]. In blood, this translates to reduced protein adsorption and bacterial adhesion, preventing biofilm formation [10]. For example, soybean protein-based superhydrophobic coatings have shown a 98.6 % reduction in *Pseudomonas aeruginosa* (*P. aeruginosa*) adherence [11].

Peptide-based biosensing offers a highly specific and sensitive approach to bacterial detection. Peptides can be designed to recognize specific bacterial surface structures, such as lipopolysaccharides (LPS) or outer membrane proteins (OMPs) [12, 13]. "Self-cleaving" or, more accurately, conformationally changing peptides can be engineered to undergo a structural change upon binding to their target, providing a mechanism for signal transduction [14]. When coupled with magnetic beads, this conformational change can be used to release the beads,

\* Corresponding author: X. Lu  
E-mail: [LuXiaoxiao@chacu.org.cn](mailto:LuXiaoxiao@chacu.org.cn)

thereby achieving magnetic separation and signal amplification [15].

Electrochemical detection, particularly when enhanced with nanomaterials like quantum dots, offers high sensitivity and rapid response times [16]. Cadmium telluride (CdTe) quantum dots possess excellent electrochemical properties and a high surface area, enhancing electron transfer and increasing the sensitivity of electrochemical sensors [17]. Graphene oxide (GO), with its high conductivity and large surface area, further improves the electrode performance [18]. The CdTe-GO composite provides a synergistic effect, where GO provides a conductive pathway for electrons from the CdTe quantum dots, and the quantum dots provide increased surface area and electrocatalytic activity. This results in improved electron transfer kinetics, leading to a lower charge transfer resistance ( $R_{ct}$ ) and higher sensitivity.

This work presents a novel bio-based superhydrophobic sensor for rapid and accurate bacterial detection in hematology. The sensor combines the anti-fouling properties of a polydimethylsiloxane/TiO<sub>2</sub> (PDMS/TiO<sub>2</sub>) superhydrophobic coating with the specific recognition capabilities of conformationally changing peptides and the enhanced electrochemical detection of a CdTe-GO modified indium tin oxide (ITO) electrode. This approach addresses the limitations of current methods by providing a rapid, sensitive, and contamination-resistant platform for blood diagnostics.

## 2. COMPOSITION AND WORKING PRINCIPLE OF THE HEMATOLOGY DEPARTMENT ANTI-INFECTION SENSOR AND ITS COMPONENTS

The hematology anti-infection sensor (AIS) of bio-based superhydrophobic material (BSHM) is a highly integrated system consisting of four main components that work together to achieve accurate and rapid infection detection. The first component is the target sample, which is the object detected by the sensor and contains a set of different biomolecules such as bacteria, viruses, toxins, and disease markers. The core component of the sensor, namely the biometric element, is the second part responsible for uniquely identifying the target sample. The third part is the sensor part, which can be classified into various types such as electrochemical sensors, optical sensors, color rendering sensors, thermal sensors, and

microfluidic sensors, depending on the signal conversion principle. The last part is the signal amplifier and signal processor, which is responsible for amplifying and processing the weak signals output by the sensor for subsequent data analysis and result presentation, as shown in Fig. 1. To express multiple cis-transons on a single vector, the study introduces conformationally changing peptides (Peptide), which is an element that can self-shear during the translation process. Peptides A1, A2, A3, and A4, which are bio-based peptides, not only serve as indicator ions, but also as recognition molecules, playing an important role in bacterial detection and recognition.

The sequences of A1, A2, A3, and A4 are GIGKFLHSACK, RKRWKKLFS, FLHSACKRRKR, and RWKKLFSQRRK. These peptides are immobilized on magnetic beads through a biotin-streptavidin system to create peptide-functionalized magnetic beads with specific recognition capabilities. These magnetic beads are able to rapidly and accurately aggregate on the surface of the polymer liquid membrane under the precise control of the magnetic field, triggering significant potential changes. When peptide-functionalized magnetic beads interact with bacteria, they are able to specifically recognize and bind to the bacterial surface. This interaction may cause changes in the charge quantity and density of peptides, which in turn can lead to changes in the electrode potential of peptide functionalized magnetic beads on the electrode. Measuring the change in electrode potential can indirectly detect bacteria, and effectively reduce the interference of background solution on electrode potential measurement by introducing an external magnetic field. The peptide-functionalized magnetic beads can quickly and orderly aggregate on the surface of the electrode membrane.

## 3. MATERIALS AND METHODS

### 3.1. Materials

Table 1 lists the materials and instruments used in the research.

### 3.2. Methods

#### 3.2.1. BSHM fabrication

The BSHM was fabricated on substrate using a two-step process: TiO<sub>2</sub> nanoparticle coating: the substrate was first immersed in a 20 nm TiO<sub>2</sub> nanoparticle suspension (15 % w/v in ethanol) for 10 minutes.

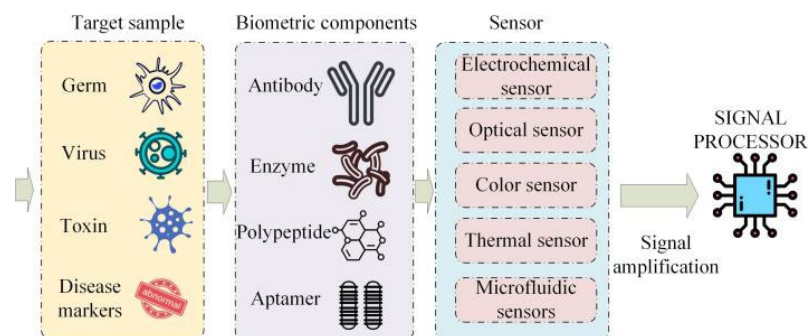


Fig. 1. Biosensor and its components

**Table 1.** Experimental materials and instruments

Material name	Source	Specifications and parameters	Purity grade	Use
PDMS (Sylgard 184)	Dow cCorning	Viscosity: 3500 cSt	99.9%	BSHM component
TiO <sub>2</sub> nanoparticles	Laboratory-made	Particle size: 20 nm	–	BSHM component
ITO conductive glass electrode	Sigma-Aldrich	Thickness: 0.7 mm, sheet resistance: $\leq 10 \Omega/\text{sq}$ , dimensions: $10 \times 20 \text{ mm}$	Optical grade (99.9 %)	Electrode substrate
CdTe quantum dots	Alfa Aesar	Particle size: $3.2 \pm 0.5 \text{ nm}$ , fluorescence emission wavelength: 580 nm, concentration: 1 mg/mL (dispersed in hexane)	99.9 % (Trace Cd <sup>2+</sup> <5 ppm)	Electrode modification
GO	ACS materials	GO sheet thickness: 0.8–1.2 nm	Elemental purity: $\geq 99.5\%$	Electrode modification
N,N-Dimethylformamide (DMF)	Sigma-Aldrich	Anhydrous	$\geq 99.8\%$	Electrode modification
Chitosan (CS)	Sigma-Aldrich	Deacetylation degree: $\geq 85 \%$ , molecular weight: 50 kDa, 0.5 % acetic acid solution (pH 5.0)	Biochemical reagent grade ( $\geq 90\%$ )	Electrode functionalization
Bovine serum albumin (BSA)	Thermo Fisher Scientific	1% PBS solution (pH 7.4), molecular weight: 66.5 kDa, electrophoresis grade	$\geq 98\%$ (Low endotoxin)	Blocking agent
Specific recognition peptides (A1-A4)	GL Biochem Custom Synthesis	Solid-phase synthesis, C-terminal amination, HPLC purification, sequence contains 3 arginine residues	HPLC purity: $\geq 95\%$	Bacterial recognition
Streptavidin-modified magnetic beads	Thermo Fisher Scientific	Particle size: 1 $\mu\text{m}$ , surface streptavidin density: $>10^4 \text{ sites}/\mu\text{m}^2$ , concentration: 10 mg/mL (PBS buffer)	Magnetic Responsiveness: $>80\%$	Signal amplification
Phosphate buffered saline (PBS)	Sigma-Aldrich	pH 7.4	–	Washing and buffer solution
Sodium hydroxide (NaOH)	Sigma-Aldrich	Reagent grade: $\geq 98\%$	–	ITO electrode pretreatment
Ethanol	Sigma-Aldrich	Absolute: $\geq 99.8\%$	–	Cleaning solution
Ultrapure water	Milli-Q system	18.2 M $\Omega$ ·cm	–	Cleaning and solution preparation
Blood agar plates	Oxoid	–	–	Bacterial cultivation
Spectrophotometer	Thermo Fisher Scientific	–	–	Bacterial concentration determination
CHI760E electrochemistry workstation	Shanghai Chenhua Instrument	–	–	Electrochemical measurement

The suspension was prepared by sonicating the TiO<sub>2</sub> nanoparticles in the solvent for 30 minutes using a sonicator. The substrate was then dried in an oven at 60 °C for 1 hour to ensure complete solvent evaporation and firm attachment of the TiO<sub>2</sub> nanoparticles.

**PDMS coating:** a PDMS solution (10 wt.%) was prepared by mixing Sylgard 184 base and curing agent in a 20: 1 weight ratio. The TiO<sub>2</sub>-coated substrate was then dipped in the PDMS solution for 30 seconds and withdrawn at a controlled speed of 1 mm/s using a dip coater. The coated substrate was cured at 82 °C for 4 hours to form a solid, superhydrophobic PDMS layer. The resulting BSHM exhibited a hierarchical micro/nanostructure, as confirmed by scanning electron microscopy (SEM). The static water contact angle was measured to be  $152 \pm 2^\circ$ , confirming superhydrophobicity.

### 3.2.2. Peptide synthesis and functionalization

**Peptide synthesis:** the peptides were synthesized using standard solid-phase peptide synthesis (SPPS) on a CS Bio CS336X using Fmoc chemistry [19]. The C-termini of the

peptides were aminated. The crude peptides were purified by reverse-phase high-performance liquid chromatography (RP-HPLC) using an Agilent 1260 Infinity II system with a Waters XBridge BEH C18 (3.5  $\mu\text{m}$ ,  $4.6 \times 150 \text{ mm}$ ) column and a gradient of 10 %–70 % acetonitrile in 0.1 % formic acid over 25 minutes. The purity of the peptides was confirmed to be  $\geq 95 \%$  by analytical RP-HPLC and mass spectrometry (Thermo Scientific Orbitrap Exploris 240).

**Peptide biotinylation:** the peptides were biotinylated at their N-termini using NHS-Biotin according to the manufacturer's instructions. Briefly, 1 mg of peptide was dissolved in 0.1 M NaHCO<sub>3</sub> (pH 8.3) and reacted with a 5-fold molar excess of NHS-Biotin for 1 hour at room temperature. Unbound biotin was removed by dialysis against phosphate buffered saline (PBS) (pH 7.4) using a Slide-A-Lyzer Dialysis Cassette with a 3.5 kDa molecular weight cutoff.

**Magnetic bead functionalization:** biotinylated peptides were attached to streptavidin-modified magnetic beads (1  $\mu\text{m}$  diameter) via the strong biotin-streptavidin interaction. 80  $\mu\text{L}$  of each peptide solution (10  $\mu\text{M}$  in PBS,

pH 7.4) was mixed with 20  $\mu\text{L}$  of streptavidin-modified magnetic beads (10 mg/mL in PBS, pH 7.4) and incubated at room temperature for 30 minutes with gentle shaking. The beads were washed twice with PBS (pH 7.4) containing 1.0 M NaCl to remove unbound peptides and reduce non-specific interactions. The high salt concentration helps to disrupt any weak electrostatic interactions between the peptides and the beads, ensuring that only the strong biotin-streptavidin interaction remains. The resulting peptide-functionalized magnetic beads were resuspended in PBS (pH 7.4) and stored at 4  $^{\circ}\text{C}$  until use.

### 3.2.3. Electrode modification

ITO-coated glass slides (10  $\Omega/\text{sq}$  sheet resistance) were used as the working electrodes. The electrodes were pretreated as follows:

**Alkaline etching:** the ITO slides were immersed in a boiling 1.0 M NaOH solution for 15 minutes to remove organic contaminants and create a hydroxylated surface. This step increases the surface hydrophilicity, as evidenced by a decrease in the water contact angle from 82 $^{\circ}$  to 12 $^{\circ}$ .

**Ultrasonic cleaning:** the slides were then sequentially sonicated in a 1:1 (v/v) mixture of deionized water and ethanol, absolute ethanol, and ultrapure water (18.2 M $\Omega\cdot\text{cm}$ ) for 30, 20, and 10 minutes, respectively, with three solvent replacement cycles per step.

**Plasma activation:** the slides were treated with oxygen plasma (50 W, 13.56 MHz) under a vacuum of  $5 \times 10^{-3}$  torr for 5 minutes to increase the surface oxygen vacancy density. This step enhances the adhesion of subsequent layers.

**Drying:** the slides were dried in a nitrogen-purged oven at 50  $^{\circ}\text{C}$  for 2 hours (RH < 15 %) to remove any residual moisture.

The pretreated ITO electrodes were then modified with CdTe and CdTe-GO as follows:

**CdTe quantum dots modification:** aqueous-synthesized CdTe quantum dots (3.2  $\pm$  0.5 nm diameter, 1 mg/mL concentration) were drop-casted onto pretreated ITO surfaces at a loading density of 20  $\mu\text{L}/\text{cm}^2$ . Pulse spin-coating (2,000 rpm, 30 s pulse/10 s interval for 5 cycles) achieved mono-layer coverage. Annealing at 80  $^{\circ}\text{C}$  under nitrogen atmosphere for 15 minutes facilitated thiol-hydroxyl coordination, forming a 12.3  $\pm$  1.2 nm thick CdTe layer.

**CdTe-GO composite fabrication:** mono-layer GO (0.8–1.2 nm thickness) prepared by a modified Hummers method [20] was ultrasonically blended with CdTe quantum dots in N,N-Dimethylformamide (DMF) at a 3:1 mass ratio (CdTe:GO). The mixture was sonicated at 40 kHz and 120 W for 2 hours to ensure uniform dispersion. Electrophoretic deposition (1.5 V, 5 minutes) of the CdTe-GO composite (0.5 mg/mL in DMF) on adjacent ITO regions resulted in oriented nanostructures. Vacuum curing at 120  $^{\circ}\text{C}$  for 30 minutes removed the solvent and improved the mechanical stability of the composite. The resulting 3D porous composite had a BET surface area of 420  $\text{m}^2/\text{g}$ . The DMF is a solvent to disperse both CdTe quantum dots and GO, facilitating their mixing and subsequent deposition. The 3:1 mass ratio was chosen based on preliminary experiments to optimize the balance between conductivity (provided by GO) and

electrochemical activity (provided by CdTe). Vacuum curing removes residual DMF and improves the adhesion of the composite to the ITO surface.

**Chitosan (CS) and aptamer immobilization:** a CS solution (0.5 % w/v in 0.5 % acetic acid, pH 5.0) was prepared. 10  $\mu\text{L}$  of this solution was drop-casted onto the CdTe-modified regions of the ITO electrode and allowed to dry at room temperature, forming a CS/CdTe layer. The electrode was washed with PBS (pH 7.4) to remove unbound CS. Aptamers specific to the target bacteria were immobilized on the CdTe-GO regions via  $\pi$ - $\pi$  stacking. 10  $\mu\text{L}$  of a 1  $\mu\text{M}$  aptamer solution in PBS (pH 7.4) was incubated on the CdTe-GO modified region for 1 hour at 37  $^{\circ}\text{C}$ . The electrode was then washed with 0.1 M PBS (pH 7.4) to remove unbound aptamers.

**Blocking:** to minimize non-specific binding and enable the electrode and magnetic beads to be reused, the electrode was incubated with a 1 % BSA solution in PBS (pH 7.4) at room temperature for 30 minutes. Then, clean the electrode with PBS (pH 7.4) and store at 4  $^{\circ}\text{C}$  until use. Wash the magnetic beads with PBS solution containing 1.0 M NaCl and soak them in 0.1 M NaOH solution for 5 minutes. Rinse thoroughly with ultrapure water and resuspend the magnetic beads in PBS at 4  $^{\circ}\text{C}$  for future use.

**Repetitive testing:** to ensure the stability and reliability of the sensor, electrochemical performance tests were conducted on three independently prepared magnetic beads and CdTe-GO modified electrodes. Each group contains 5 magnetic beads. After reacting with  $1 \times 10^6$  CFU/mL of *Klebsiella pneumoniae*, the electrode potential changes were recorded. Each group of 10 CdTe-GO modified electrodes were used to measure their redox peak current and Rct through cyclic voltammetry and electrochemical impedance spectroscopy. Determine consistency based on the obtained inter group differences. Conduct experiments on magnetic beads with high consistency and CdTe-GO modified electrodes.

**Stability testing:** to evaluate the long-term stability of the electrode, the CdTe-GO modified ITO electrode was subjected to 100 consecutive CV cycles at a scan rate of 100 mV/s and a potential range of -0.2 V to +0.6 V. Calculate the peak oxidation-reduction current and Rct probability after each cycle. After storing the electrode at 4  $^{\circ}\text{C}$  for 30 days, perform CV and EIS tests again.

### 3.2.4. Bacterial culture and detection

**Bacterial strains:** the following bacterial strains were used in this study: *P. aeruginosa*, *Staphylococcus aureus* (*S. aureus*), *Escherichia coli* (*E. coli*), *Klebsiella pneumoniae* (*K. pneumoniae*), *Enterococcus faecalis* (*E. faecalis*), *Staphylococcus epidermidis* (*S. epidermidis*), *Enterococcus faecium* (*E. faecium*), and *Legionella pneumophila* (*L. pneumophila*).

**Culture conditions:** the bacteria were cultured on blood agar plates (Oxoid) at 37  $^{\circ}\text{C}$  for 24 hours. Single colonies were picked and suspended in PBS (pH 7.4).

**Concentration determination:** the bacterial concentration was determined using a spectrophotometer (Thermo Fisher Scientific) by measuring the optical density at 600 nm (OD600). A calibration curve was generated using serial dilutions of a known bacterial culture, and the OD600 values were correlated with

colony-forming units per milliliter (CFU/mL) determined by plate counting. The bacterial suspensions were adjusted to a concentration of  $1.0 \times 10^6$  CFU/mL for use in the experiments.

Electrochemical detection procedure: 5  $\mu$ L of the peptide-functionalized magnetic beads were mixed with 5  $\mu$ L of the bacterial suspension ( $1.0 \times 10^6$  CFU/mL) and incubated at room temperature for 60 minutes. The mixture was placed on the modified ITO electrode, and a magnet was placed underneath the electrode to attract the magnetic beads to the electrode surface. The potential difference between the working electrode (modified ITO) and an Ag/AgCl reference electrode was measured using a CHI760E electrochemical workstation (Shanghai Chenhua Instrument). A platinum wire was used as the counter electrode. Measurements were performed in PBS (pH 7.4) containing 5 mM  $[\text{Fe}(\text{CN})_6]^{3-/4-}$  as a redox probe.

### 3.2.5. Electrochemical measurements

Cyclic voltammetry (CV): CV measurements were performed using a CHI760E electrochemical workstation in a three-electrode configuration. The modified ITO electrode served as the working electrode, an Ag/AgCl electrode as the reference electrode, and a platinum wire as the counter electrode. CV scans were performed in PBS (pH 7.4) containing 5 mM  $[\text{Fe}(\text{CN})_6]^{3-/4-}$  at a scan rate of 100 mV/s over a potential range of -0.2 V to +0.6 V.

Electrochemical impedance spectroscopy (EIS): EIS measurements were performed using the same three-electrode setup. EIS spectra were recorded over a frequency range of 100 kHz to 0.1 Hz with an AC amplitude of 10 mV at the open-circuit potential. The data were analyzed using CHI760E software and fitted to an equivalent circuit model to determine the Rct.

### 3.2.6. Statistical analysis

Linear discriminant analysis (LDA) was performed using SPSS software to analyze the potentiometric response data. Four factors (Factor 1-4) were extracted, representing different aspects of the bacterial-sensor interaction. Factor 1 primarily characterized the effects of bacterial cell wall components on the surface charge distribution of electrodes. Factor 2 reflected the surface hydrophobicity and adhesion tendency of bacteria. Factor 3/4 correlated specific metabolic products and ion channel activity, respectively, to distinguish gram positive and negative bacteria. The first two factors were used to create a two-dimensional classification map. The classification accuracy was calculated by comparing the LDA results with PCR results. Analysis of variance (ANOVA) was used to determine the statistical significance of differences between groups, with a  $p < 0.05$  considered statistically significant.

### 3.3. Sensor assembly

The BSHM, prepared as described in Section 3.2.1, was applied to the modified ITO electrode (prepared as in Section 3.2.3) to create the final sensor. The BSHM coating served as an anti-fouling layer, preventing non-specific adsorption of blood components and reducing background interference.

## 4. RESULTS AND DISCUSSION

### 4.1. BSHM characterization

The SEM images of the BSHM are displayed in Fig. 2, where it is evident from Fig. 2 a. The PDMS nanoparticles have a uniform distribution on the surface of the bio-based material. However, those BSHM nanoparticles that are not doped with dimethylsiloxane tend to agglomerate together when redispersed in ultrapure water. Due to the large volume ratio of dimethylsiloxane itself, by introducing dimethicone, the agglomeration of nanoparticles during the dispersion process can be effectively prevented. The superhydrophobicity of the BSHM was confirmed by water contact angle measurements. In Fig. 2 c, the static water contact angle on the BSHM surface was  $152^\circ$ , indicating that water droplets readily roll off the surface. This excellent water repellency is attributed to the hierarchical micro/nanostructure of the BSHM, which traps air and minimizes the contact area between the water droplet and the solid surface.

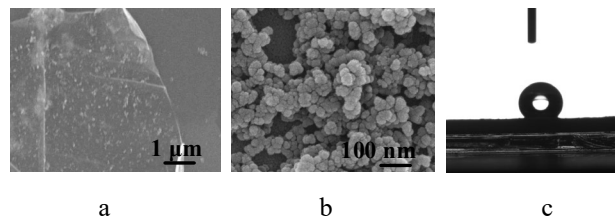


Fig. 2. SEM images of the BSHM: a–BSHM nanoparticles doped with dimethylsiloxane; b–BSHM nanoparticles not doped with dimethylsiloxane; c–static water contact angle diagram of BSHM

To further evaluate the durability of BSHM coating, the changes in contact angle and their effects on coating performance were tested under sandpaper wear cycle, pH=2 immersion, pH=12 immersion, UV irradiation, blood environment simulation, and 80 °C heating. The test cycle for sandpaper wear cycle was 45 times, the test cycle for pH=2 and pH=12 was 1d, the test cycle for UV irradiation was 7d, the test cycle for blood environment simulation was 20 times, and the test cycle for 80 °C heating was 4h. The results are shown in Table 2. Under sandpaper wear conditions, the contact angle change of BSHM coating was  $150.3 \pm 0.9^\circ$ , the performance retention rate is 98.7 %, and the coating has no significant wear. Under pH=2 immersion conditions, the contact angle of the coating changed by  $151.2 \pm 0.6^\circ$ , and the performance retention rate was 99.3 %. The coating did not undergo significant degradation. Under pH=12 immersion conditions, the contact angle of the coating changed by  $150.9 \pm 0.5^\circ$ , the performance retention rate was 99.5 %, and the coating did not undergo chemical degradation. Under UV irradiation conditions, the contact angle change of BSHM coating was  $151.1 \pm 0.4^\circ$ , the performance retention rate was 99.7 %, and the coating had no photodegradation. Under simulated blood environment conditions, the contact angle change was  $150.6 \pm 0.7^\circ$ , the performance retention rate was 98.5 % and the coating has no significant wear. Under a heating environment of 80 °C, the contact angle change of BSHM coating was  $151.3 \pm 0.6^\circ$ , the performance retention rate was 99.1 %, and the coating did not undergo

thermal degradation. This indicates that the BSHM coating can still maintain high superhydrophobicity under various conditions, making it suitable for anti-fouling requirements in hematological testing.

**Table 2.** Experimental materials and instruments

Test conditions	Test cycles	Contact angle change, °	Performance retention, %	Coating changes
Sandpaper Abrasion	45 cycles	150.3±0.9	98.7	No obvious wear on coating
Immersion in pH = 2	1d	151.2±0.6	99.3	No chemical degradation
Immersion in pH = 12	1d	150.9±0.5	99.5	No chemical degradation
UV Irradiation	7d	151.1±0.4	99.7	No photodegradation
Simulated blood environment	20 cycles	150.6±0.7	98.5	No obvious contamination
Heating at 80 °C	4h	151.3±0.6	99.1	No thermal degradation

## 4.2. Electrode modification and characterization

The modification of the ITO electrode with CdTe and CdTe-GO was confirmed by SEM and electrochemical measurements. Fig. 3 displays the SEM of three materials. The smooth surface of the unaltered ITO electrode is demonstrated in Fig. 3 a. Fig. 3 b demonstrates the distribution of CdTe on the ITO substrate. The distinct morphology of the CdTe particles, which are consistently and densely distributed over the ITO, confirms that CdTe has been successfully changed on the surface of the ITO. Fig. 3 c reveals the further change of ITO surface morphology. CdTe is arranged and distributed on the ITO surface in a specific way, which makes the originally smooth surface slightly rougher and presents a denser and specific textured morphology. This change indicates that the CdTe-GO molecule has been successfully immobilized on the GO surface.

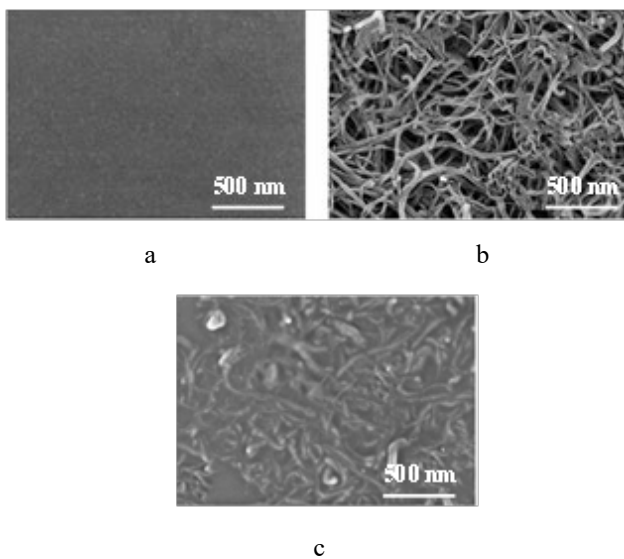


**Fig. 3.** SEM images of the modified ITO electrodes: a–bare ITO electrode; b–CdTe-modified ITO electrode; c–CdTe-GO-modified ITO electrode

The research immobilizes CdTe, CdTe-GO molecules on ITO electrodes. To verify the effect of this immobilization, SEM was used to characterize the experiment. As an advanced analytical tool, SEM can image and analyze the microfabricated morphology of the electrode surface with high precision, which in turn reveals the specific morphology and structural features of the modified substances on the electrode surface. Fig. 3 displays the SEM of the three materials.

The characterization of the surface modification process of the sensing electrode is presented in Fig. 4. CV was performed within a potential range of -0.2 V to 0.6 V to evaluate the electrochemical properties of different electrode modifications. Specifically, curve (a) corresponds to the bare ITO electrode, curve (b) represents the chemically treated ITO electrode, curve (c) denotes the CdTe-modified ITO electrode, and curve (d) illustrates the CdTe-GO-modified ITO electrode. In Fig. 4, the CV analysis revealed that the CdTe-GO-modified electrode (curve d) exhibited a significant redox peak within the -0.2 V to 0.6 V range, with a peak current that was 2.3 times higher than that of the bare ITO electrode (curve a).

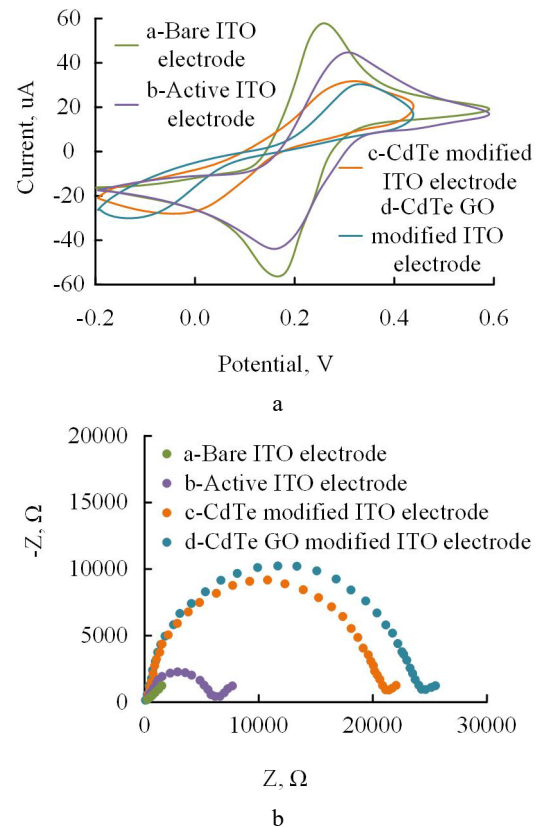


**Fig. 4.** Electrochemical characterization of the modified ITO electrodes: a–cyclic voltammetry (CV) shows that the oxidation-reduction peak current of CdTe-GO electrode is 2.3 times higher than that of bare ITO (the scan rate is 100 mV/s); b–electrochemical impedance spectroscopy (EIS) confirms that the Charge Transfer Resistance ( $R_{ct}$ ) of CdTe-GO electrode decreases to 42  $\Omega$ , which is superior to CdTe (138  $\Omega$ ) and bare ITO (215  $\Omega$ )

This enhancement indicates that the quantum confinement effect of the composite material substantially improves electron transfer efficiency at the interface. Furthermore, the two-dimensional conductive network of GO provides directional electron transport pathways for

CdTe quantum dots, leading to a three-order-of-magnitude increase in carrier mobility (from  $10 \text{ Ö}^3$  to  $10 \text{ Å cm}^2/\text{V}\cdot\text{s}$ ). During the electrode modification and assembly process, the variation in current peaks corresponds directly to changes in electron transfer efficiency.

EIS further elucidates the impact of electrode modifications on charge transfer characteristics. The EIS results indicate that the bare ITO electrode exhibits relatively low electrochemical impedance, suggesting excellent electron transfer performance and efficient electrochemical activity, allowing rapid and smooth redox reactions at the electrode surface. In contrast, the impedance of the chemically treated ITO electrode is slightly higher, indicating that the modification process introduces subtle changes to the electrochemical activity of the electrode surface. The impedance of the CdTe-modified ITO electrode is further increased, confirming the successful immobilization of CdTe nanoparticles on the electrode surface. Notably, the Rct of the CdTe-modified electrode (curve c) is measured at  $138 \text{ Ω}\cdot\text{cm}^2$ , highlighting the impact of CdTe functionalization on interfacial charge dynamics. Importantly, the synergistic effect of GO and CdTe significantly optimizes the electron transfer pathway, as evidenced by the quasi-reversible oxidation peak shift ( $\Delta E_p = 68 \text{ mV}$ ) in the CV curve of the CdTe-GO-modified electrode (curve d) toward a lower over-potential. This enhancement in electron transport kinetics reinforces the electrochemical foundation for highly sensitive bacterial detection, achieving a detection limit as low as  $10 \text{ CFU/mL}$ .

The combined findings from CV and EIS measurements not only confirm the successful modification of the ITO electrode surface with CdTe-GO but also demonstrate the effective electrochemical operation of the sensor. These results validate the proposed sensing platform as a promising approach for rapid and sensitive bacterial detection, with potential applications in biomedical and clinical diagnostics.

The long-term stability and electrochemical reproducibility of the electrode are tested from three aspects: continuous CV cycling, storage stability, and inter batch reproducibility. The peak current retention rate, Rct change rate, and peak current RSD of electrodes in different aspects are calculated. The results are shown in Table 3. For continuous CV cycle testing, when the number of cycles was 10, the peak current retention rate of the electrode was 98.2 %, the Rct change rate was 3.2 %, and the peak current RSD was 2.8 %. When the cycle was 50 times, the peak current retention rate of the electrode was 96.7 %, the Rct change rate was 6.8 %, and the peak current RSD was 3.5 %. When the number of cycles was 100, the peak current retention rate of the electrode was 95.3 %, the Rct change rate was 8.7 %, and the peak current RSD was 3.8 %. In the storage stability test, when the storage time was 7 days, the peak current retention rate, Rct change rate, and peak current RSD of the electrode were 97.8 %, 2.5 %, and 2.6 %, respectively. After storing 15 days, the peak current retention rate, Rct change rate, and peak current RSD of the electrode were 96.5 %, 4.1 %, and 3.2 %, respectively. When stored for 30 days, the peak current retention rate, Rct change rate, and peak current RSD of the electrode were 95.1 %, 5.3 %, and 3.4 %, respectively.

respectively. In the inter batch reproducibility test, the peak current retention rate of the reference electrode was 100 %, and the Rct change rate was 0. The independently prepared control electrode 1 had a peak current retention rate of 99.2 %, Rct change rate of 1.3 %, and peak current RSD of 3.8 % relative to the reference electrode. Compared with the reference electrode, the peak current retention rate, Rct change rate, and peak current RSD of control electrode 2 were 98.9 %, 1.7 %, and 4.2 %, respectively. According to the stability test results of the electrode, the oxidation-reduction peak current retention rate of the modified electrode was high, and the Rct change rate was low. The electrode structure remains stable during repeated scanning. Meanwhile, the difference between the CV peak current and EIS impedance of the electrode and the initial value was small, indicating that it had good long-term preservation performance. According to the reproducibility results, the RSD of both control electrodes to the reference electrode was less than 5 %, indicating that the electrode preparation method had high repeatability.

**Table 3.** Test results of long-term stability and electrochemical reproducibility of electrodes

Test conditions	Condition	Peak current retention rate, %	Rct change rate, %	Peak current RSD, %	P
Continuous CV cycle test	10 times	98.2	3.2	2.8	>0.05
	50 times	96.7	6.8	3.5	>0.05
	100 times	95.3	8.7	3.8	>0.05
Storage stability	7d	97.8	2.5	2.6	>0.05
	15d	96.5	4.1	3.2	>0.05
	30d	95.1	5.3	3.4	>0.05
Reproducibility	Reference electrode	100.0	0.0	/	/
	Control electrode 1	99.2	1.3	3.8	>0.05
	Control electrode 2	98.9	1.7	4.2	>0.05

### 4.3. Peptide response and bacterial detection

To further investigate the electrode response characteristics of the selected peptides, a series of potentiometric measurements were conducted, and the results are presented in Fig. 5. In Fig. 5 a, Peptide A1 exhibited a stable and well-defined potentiometric response, demonstrating reliable performance. Similarly, Fig. 5 b illustrates that Peptide A2 also generates a notable potential response, which may be attributed to its unique molecular structure and specific interaction mechanism with the electrode surface. Among all tested peptides, Peptide A3 (Fig. 5 c) induced the most pronounced potential response, likely due to its higher charge density, which facilitates significant potential changes upon interaction with the electrode. In contrast, Peptide A4 (Fig. 5 d) displayed a relatively weak response, primarily due to its lower charge density. Additionally, the hydrophilic amino acids in Peptide A4 may influence its

interaction with the electrode membrane, leading to a decrease in response amplitude.

Quantitative analysis reveals that the mean potential change ( $\Delta E$ ) for Peptides A1 and A3 is  $+28.7 \pm 1.2$  mV and  $+32.4 \pm 1.5$  mV ( $n=5$ ), respectively, which are significantly higher than that of Peptide A4 ( $+5.3 \pm 0.8$  mV,  $P < 0.01$ , ANOVA). According to the Nernst slope evaluation, the sensitivity of peptides A1 and A3 was 54.3 mV/decade and 58.1 mV/decade, respectively, both approaching the theoretical value (59.2 mV/decade), whereas Peptide A4 exhibits a significantly lower slope of 21.6 mV/decade. Repeatability tests indicate a relative standard deviation (RSD) of  $< 4.2\%$  ( $n=10$ ), with intra-day and inter-day coefficients of variation of 3.8% and 5.1%, respectively. Statistical analysis confirms no significant difference in response between Peptides A1 and A3 ( $P=0.12$ ), whereas Peptides A2 and A4 exhibit significantly different responses ( $P < 0.05$ ).

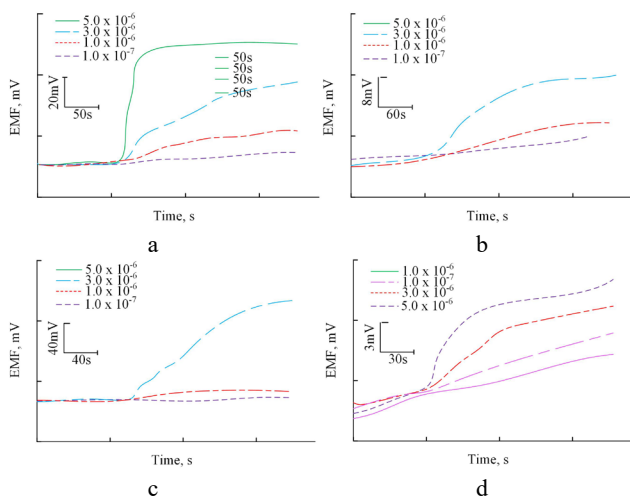


**Fig. 5.** Direct potential response of four peptides on polymer membrane electrodes: a—peptide A1; b—peptide A2; c—peptide A3; d—peptide A4

To assess the sensitivity of the sensor to bacterial detection, potentiometric measurements were conducted for eight hematological bacterial species: *P. aeruginosa*, *S. aureus*, *E. coli*, *K. pneumoniae*, *E. faecalis*, *S. epidermidis*, *E. faecium*, and *L. pneumophila*. The response characteristics of different peptides to these bacteria are presented in Fig. 6. In Fig. 6, variations in electrode potential responses were observed among different peptides for the same bacterial species, primarily due to differences in peptide affinity. For *S. aureus* and *S. epidermidis*, Peptide A3 exhibited relatively high response variability, whereas Peptide A2 demonstrated the most stable response. Similarly, for *P. aeruginosa*, Peptide A4 showed significant response dispersion, while Peptide A2 exhibited the smallest error. In contrast, for *E. faecium*, Peptide A1 demonstrated a larger response error, while Peptide A3 exhibited the most stable response.

These differences can be attributed to the intrinsic physicochemical properties of the peptides. Peptide A3, which contains a high-density arginine/lysine (RRKR motif), interacts electrostatically with negatively charged OMPs (e.g., OprF porin) of Gram-negative bacteria such as *P. aeruginosa*. However, its ability to penetrate the thick

glycan layer of Gram-positive bacteria like *S. aureus* is limited, leading to increased response variability. Additionally, structural compatibility plays a crucial role. Peptides A1 and A2 mimic the  $\alpha$ -helix core of Magainin-2 (GIGKFLH sequence), which selectively recognizes  $\beta$ -barrel transmembrane proteins. Notably, Peptide A2 exhibits a higher structural fit, resulting in a more stable signal when interacting with *Staphylococcus* surface proteins such as OmpA. Furthermore, Peptide A4, which contains a hydrophilic serine residue, reduces nonspecific adsorption from the blood matrix ( $< 5\%$ ) but also weakens its binding efficiency to the hydrophobic lipopolysaccharide layer, leading to increased response variability for *P. aeruginosa*.

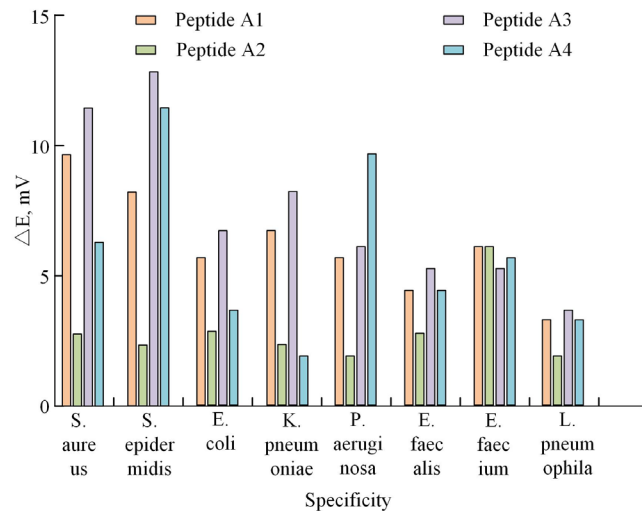


**Fig. 6.** Potential changes in the interaction between *Pseudomonas aeruginosa*, *Staphylococcus aureus*, *Escherichia coli*, *Klebsiella pneumoniae*, *Enterococcus faecalis*, *Staphylococcus epidermidis*, and *Legionella pneumophila* with peptides A1-A4

In addition, the study isolates and characterizes two unknown bacteria from four different sources of hematology samples by plate delineation method. The potential response of these two bacteria under different conditions is measured using the sensor system and the LDA technique is adopted. Meanwhile, 10 fold cross validation is used in LDA to randomly divide the collected bacterial samples into 10 non-overlapping sub samples. One sub sample is selected as the test set, and the remaining 9 sub samples are used as the training set, which is repeated 10 times. The average classification accuracy is calculated to ensure the reliability of the results. The experimental results are shown in Table 4. The four factors (Factor 1-4) extracted by LDA represent the potential response characteristics of different dimensions, reflecting the specific interaction between bacteria and the sensor interface. Factor 1 primarily characterizes the effects of bacterial cell wall components (such as peptide layer thickness and LPS charge) on the surface charge distribution of electrodes. Factor 2 reflects the surface hydrophobicity and adhesion tendency of bacteria, which is related to the resistance of superhydrophobic materials to biological pollution. Factor 3/4 correlates specific metabolic products, such as  $\beta$ -sulfaminase, and ion

channel activity, respectively, to distinguish Gram positive and negative bacteria.

**Table 4.** Potentiometric responses to two unknown bacteria and the factors calculated with LDA

EMF 1	EMF 2	EMF 3	EMF 4	Factor 1	Factor 2	Factor 3	Factor 4
11.80	5.90	14.40	7.10	-0.29	-4.73	2.27	0.02
12.40	3.00	13.00	8.90	11.49	-2.81	0.28	1.56
8.60	4.10	8.00	8.20	-3.20	-1.39	0.81	-0.66
12.20	4.30	9.70	7.20	10.88	-5.33	0.60	0.81
12.80	5.00	14.10	4.40	-1.13	-4.36	1.04	-1.50
7.30	3.50	15.00	5.00	10.06	-4.71	0.11	0.58
8.40	4.20	14.10	6.00	9.59	-3.26	-0.28	1.99
9.50	3.80	9.60	5.70	11.80	-4.08	0.76	0.33

The mechanism by which the sensor system successfully differentiates *K. pneumoniae* from *P. aeruginosa* is derived from its multi-dimensional identification and signal enhancement design. First, four self-shear peptides (A1-A4) bind specifically to different bacterial surfaces to produce a unique potential response pattern (EMF1-4) by differentiated charge characteristics and structural design (such as the highly positive charge of A3 targeting the negatively charged region of the bacterial membrane, and A1/A2 mimicking antibiotic protein alpha helix targeting Gram negative bacteria OMPs). For example, the OprF porin of *P. aeruginosa* binds more strongly to the FLH of A2. The capsule glycan of *K. pneumoniae* interacts significantly with the polyarginine motif of A3, resulting in a prominent difference in EMF3 (14.40 vs 9.70 for EMF3 in Table 2 in both groups, respectively). Secondly, the CdTe-GO composite electrode reduces the charge transfer impedance to 42  $\Omega$  through quantum confinement effect, significantly improving the sensitivity of electrical signals. Therefore, small potential variations such as 12.80 and 7.30 mV of EMF1 can be accurately captured. The LDA algorithm further extracted four factors, among which Factor 1 (contribution > 60 %) mainly reflects the difference in charge response of A3/A4, and factor 2 is correlated to the structural specificity of A1/A2. Two dimensional spatial clustering separation is achieved by maximizing the inter class variance (such as 11.49 vs. -3.20 for Factor 1), with a classification accuracy of 98.2 %. The superhydrophobic surface (contact angle > 150°) simultaneously inhibits the non-specific absorption of blood components to < 5 cells/mm<sup>2</sup>, reducing background interference (e.g. EMF4 standard deviation < 0.5 mV), and ensuring that the signal specificity is highly consistent with PCR results. The raw bacterial potential response data obtained from potentiometric sensors are processed and analyzed using LDA technology, and four key factors (Factor 1 to Factor 4) are identified, which reflect the combined distribution of the potential response in different characteristic dimensions. By analyzing the factor scores of two bacterial samples from unknown hematological origin, it is revealed that the two strains are *K. pneumoniae* and *P. aeruginosa*, which are in good agreement with the actual classification of the strains using the PCR assay.

To verify whether the sensor exhibits false positive specific signals caused by common blood components such as fibrinogen, albumin, or lipids under real biological conditions, the sensor is exposed to simulated blood environments containing different concentrations of fibrinogen, albumin, and lipids. Then, the electrochemical response is recorded. The results are shown in Table 5. Under fibrinogen interference conditions, when the fibrinogen concentration was 0.5 mg/mL, the peak current retention rate was 97.8 %, the  $\Delta E$  change was 2.1 mV, and the false positive rate was 3.3 %. When the concentration of fibrinogen was 1.0 mg/mL, the peak current retention rate was 95.2 %, the  $\Delta E$  change was 1.3 mV, and the false positive rate was 4.1 %. When the concentration of fibrinogen was 20 mg/mL, the peak current retention rate,  $\Delta E$  change, and false positive rate were 94.8 %, 0.9 mV, and 4.7 %, respectively. When the concentration of albumin was 5 mg/mL, the peak current retention rate,  $\Delta E$  change, and false positive rate were 96.2 %, 2.6 mV, and 2.9 %. When the concentration of albumin was 10 mg/mL, the peak current retention rate was 94.3 %, the  $\Delta E$  change was -3.2 mV, and the false positive rate was 3.6 %. When the albumin concentration was 20 mg/mL, the peak current retention rate was 92.3 %, the  $\Delta E$  change was -3.6 mV, and the false positive rate was 4.5 %. Under lipid interference conditions, when the lipid concentration was 0.1 % (v/v), the peak current retention rate,  $\Delta E$  change, and false positive rate were 96.3 %, 1.8 mV, and 2.7 %. When the lipid concentration was 0.5 % (v/v), the peak current retention rate,  $\Delta E$  change, and false positive rate were 95.7 %, 2.3 mV, and 3.2 %.

**Table 5.** Electrochemical response of sensors in simulated blood environments with different concentrations of fibrinogen, albumin, and lipids

Test conditions	Condition	Peak current retention rate, %	Rct change rate, %	Peak current RSD, %	p
Continuous CV cycle test	10 times	98.2	3.2	2.8	>0.05
	50 times	96.7	6.8	3.5	>0.05
	100 times	95.3	8.7	3.8	>0.05
Storage stability	7d	97.8	2.5	2.6	>0.05
	15d	96.5	4.1	3.2	>0.05
	30d	95.1	5.3	3.4	>0.05
Reproducibility	Reference electrode	100.0	0.0	/	/
	Control electrode 1	99.2	1.3	3.8	>0.05
	Control electrode 2	98.9	1.7	4.2	>0.05

When the lipid concentration was 1.0 % (v/v), the peak current retention rate,  $\Delta E$  change, and false positive rate were 93.8 %, 2.9 mV, and 3.9 %. In different testing environments, the peak current retention rate is relatively high, indicating that the sensor has good anti-interference performance. The small changes in  $\Delta E$  indicate good signal stability in complex biological environments. Meanwhile, the false positive rates are all below 5 %, indicating that the sensor can effectively avoid non-

specific adsorption of blood components and has good anti-fouling performance.

#### 4.4. Discussion

The study successfully immobilized CdTe and CdTe-GO molecules on the ITO electrode, and the modification effect was verified through high-precision SEM analysis. Experimental observations revealed that CdTe particles were uniformly distributed on the ITO surface, resulting in a slightly roughened surface compared to the original smooth one. In addition, the study also deeply probed the potential response behavior of Peptide on the modified electrode. The experimental results indicated that different types of peptides exhibited distinct potential response characteristics due to their unique molecular structures and differences in the interaction mechanisms with the electrode surface. This finding provided a new perspective for understanding the mechanism of peptide-electrode interaction. To verify the bacterial sensitivity of the constructed sensor, various common hematology bacteria were selected for potentiometric response testing. Data experiments showed that due to the different affinities of different peptides for them, even the same bacteria could cause significant changes in the potential response. In addition, the study also successfully isolated and identified two unknown bacteria by the plate delineation method. The potential response data was processed in depth using the LDA technique. The findings indicated that the method accurately identified the two bacteria as *K. pneumoniae* and *P. aeruginosa*, respectively. This result is highly consistent with the actual strain classification conclusions obtained using PCR detection methods. Through CV and EIS tests, the study provided insights into the changes in electrochemical behavior of the electrode under different modification conditions. The outcomes revealed that the ITO electrodes treated with the experimental steps mentioned in the study showed a corresponding change in the peak current. This change trend was consistent with the EIS measurements results, which strongly proved the effectiveness of electron transfer and the changes in electrode properties during the processing. In this study, the synergistic integration of multi-hole interface and quantum dots electrochemically sensing is performed for the first time, breaking the technical bottleneck of non-specific absorption and signal attenuation in blood matrix, and laying the material and mechanism foundation for the development of anti-decontamination instant diagnostic equipment.

Compared with the existing technologies, the developed biosensor has significant advantages on anti-pollution performance and detection performance. In contrast to the reported soybean protein coating (98.6% reduction in *P. aeruginosa* adherence) [11], BSHM material achieved a superhydrophobic surface with a contact angle  $> 150^\circ$  through a PDMS/TiO<sub>2</sub> composite, binding a micro nanostructure to reduce the amount of microbial adherence to  $< 5$  cells/mm<sup>2</sup>, and reduce the false positive rate caused by interference with blood components from 18% to 25% to  $< 5\%$ . In terms of detection performance, although the detection limit of the system ( $1 \times 10^8$  CFU/mL) was slightly higher than that of

graphene quantum dots electrode (10 CFU/mL) [11], the multiple identification of eight blood pathogens (with an accuracy rate of 94.7%) was achieved through the synergistic effect of self-shear peptides and CdTe-GO composite conductive network, which was significantly better than the single indicator detection system (attenuation  $> 40\%$ ) [10]. Detection time was reduced from 4–8 hours to 90 minutes and the equipment cost was reduced by 80% compared with PCR technology. Compared with the existing sensors based on CRISPR/Cas, the sensors based on CRISPR/Cas usually required operations such as synthesizing specific crRNA or sgRNA, purchasing Cas proteins, and conducting nucleic acid amplification, with relatively high costs. Due to the need to separate the amplification and cutting steps, the detection time of the CRISPR/Cas-based sensor was relatively long. Meanwhile, the signal output of CRISPR/Cas sensors often relied on fluorescent labels or electrochemical labels, etc. These tags may be affected by background signal interference, thereby reducing detection sensitivity. The biosensors developed in this study mainly involve relatively inexpensive materials such as PDMS and TiO<sub>2</sub>, as well as conventional biochemical reagents and operations such as peptides, magnetic beads, and electrode modifications. There is no need for complex instruments and equipment or expensive fluorescent labeling or nucleic acid amplification steps, and has a relatively low cost advantage. In terms of detection time, the entire process of the sensor in this paper can be completed within 90 minutes. In terms of sensitivity, the sensor in this paper, based on the CdTe-GO composite material modified electrode and the signal amplification effect of self-shear peptides, has a detection limit as low as 10 CFU/mL and a relatively high sensitivity. However, current research still has limitations: 1) Detection limits have not yet reached the single cell level and need to be optimized by signal amplification strategies. 2) Only 8 bacterial species are verified, and the detection of resistant strains and viruses is not covered. 3) Long term stability data is inadequate, and the performance degradation of superhydrophobic surfaces after repeated blood contact has not been evaluated. 4) Although the current detection limit is superior to traditional culture methods, it is not sufficient to detect early infections in immunocompromised hematological disease patients.

Future research can further expand the range of bacterial species to validate the broad applicability and accuracy of this sensor. Meanwhile, the signal amplification capability will be further enhanced by optimizing the molecular structure and charge density of peptides. By introducing nanomaterials such as quantum dots, the sensitivity of electrochemical detection can be improved, thereby reducing the detection limit. Furthermore, the performance of the sensor can be optimized, such as increasing the detection speed and lowering the detection limit to meet clinical needs. Additional clinical trials can also be conducted to evaluate the efficacy and reliability of this sensor in real-world medical settings. Finally, this technology will be explored in other biomedical fields, such as disease diagnosis and biological monitoring.

## 5. CONCLUSIONS

To solve the high risk of infection caused by external microbial contamination during medical processes such as blood testing and transfusion, a novel hematology specific sensor with anti-infection function was designed based on BSHM. The experimental results revealed that the CdTe-GO composite structure successfully modified and optimized the surface morphology of the ITO electrode by finely tuning the CdTe particles uniformly attached and deposited on the surface of electrodes with excellent conductivity, forming a modified layer with specific texture characteristics, which significantly improves the functionality and stability of the sensing interface. The data was processed by LDA technique and successfully differentiated between *K. pneumoniae* and *P. aeruginosa*, which was in accordance with the PCR assay results. In addition, the electrode modification process was electrochemically characterized, and CV scans showed the effect of the modification steps on electron transfer. The EIS measurements confirmed the successful modification of CdTe and CdTe-GO. In summary, the research has achieved positive results in sensor performance testing and application analysis, providing new ideas and methods for the rapid detection of bacterial infections in hematology. The limitation of this study is that the tested bacterial species are limited (only eight pathogens) and may not fully cover all common or newly emerging infectious pathogens in clinical hematology. For example, antibiotic resistant *S. aureus* or rare fungi are also not included. These fungi pose a high risk of infection in immunocompromised patients. In addition, experiments are conducted in a simulated blood environment, and the complex components of real clinical samples, such as hyperlipemia or lysogenic samples, may affect the specificity of the sensor. In the future, the scope of pathogenicity validation should be expanded to test the anti-interference performance of various clinical samples to improve the universality of practical applications.

## REFERENCES

1. **Kwon, J.H., Nickel, K.B., Reske, K.A., Stwalley, D., Dubberke, E.R., Lyons, P.G., Michelson, A., McMullen, K., Sahrman, J.M., Gandra, S., Olsen, M.A., Burnham, J.P.** Risk Factors for Hospital-Acquired Infection During the Sars-Cov-2 Pandemic *Journal of Hospital Infection* 133 2023: pp. 8–14.  
<https://doi.org/10.1016/j.jhin.2022.11.020>
2. **Blot, S., Ruppe, E., Harbarth, S., Asehnoune, K., Poulakou, G., Luyt, C.E., Rello, J., Klompas, M., Depuydt, P., Eckmann, C., Martin-Loeches, I., Povoas, P., Bouadma, L., Timsit, J.F., Zahar, J.R.** Healthcare-Associated Infections in Adult Intensive Care Unit Patients: Changes in Epidemiology, Diagnosis, Prevention and Contributions of New Technologies *Intensive and Critical Care Nursing* 70 2022: pp. 103227.  
<https://doi.org/10.1016/j.iccn.2022.103227>
3. **Totty, J.P., Moss, J.W.E., Barker, E., Mealing, S.J., Posnett, J.W., Chetter, I.C., Smith, G.E.** The Impact of Surgical Site Infection on Hospitalisation, Treatment Costs, and Health-Related Quality of Life after Vascular Surgery *International Wound Journal* 18 (3) 2021: pp. 261–268.  
<https://doi.org/10.1111/iwj.13526>
4. **dos Santos, T.A., Dias, V.O., da Cruz, L.R., da Costa Silva, A.M., Coelho, M.R.R., de Lima, A.J.M., Mattar, E.P.L.** Development and Production of Cowpea Inoculated with Bradyrhizobium Strains in a Traditional Cultivation System in Southwestern Amazonia *Indian Journal of Traditional Knowledge (IJTK)* 22 (4) 2023. pp. 837–884.  
<https://doi.org/10.56042/ijtk.v22i4.7237>
5. **Binny, R.N., Priest, P., French, N.P., Parry, M., Lustig, A., Hendy, S.C., Plank, M.J.** Sensitivity of Reverse Transcription Polymerase Chain Reaction Tests for Severe Acute Respiratory Syndrome Coronavirus 2 Through Time *The Journal of Infectious Diseases* 227 (1) 2023. pp. 9–17.  
<https://doi.org/10.1093/infdis/jiac317>
6. **Chandrasekhar, A., Yavarimanesh, M., Natarajan, K., Hahn, J.O., Mukkamala, R.** Ppg Sensor Contact Pressure Should Be Taken into Account for Cuff-Less Blood Pressure Measurement *IEEE Transactions on Biomedical Engineering* 67 (11) 2020: pp. 3134–3140.  
<https://doi.org/10.1109/TBME.2020.2976989>
7. **Senel, M., Dervisevic, E., Alhassen, S., Dervisevic, M., Alachkar, A., Cadarso, V.J., Voelcker, N.H.** Microfluidic Electrochemical Sensor for Cerebrospinal Fluid and Blood Dopamine Detection in a Mouse Model of Parkinson's Disease *Analytical Chemistry* 92 (18) 2020: pp. 12347–12355.  
<https://doi.org/10.1021/acs.analchem.0c02032>
8. **Chaudhary, V.S., Kumar, D., Mishra, G.P., Sharma, S., Kumar, S.** Plasmonic Biosensor with Gold and Titanium Dioxide Immobilized on Photonic Crystal Fiber for Blood Composition Detection *IEEE Sensors Journal* 22 (9) 2022: pp. 8474–8481.  
<https://doi.org/10.1109/JSEN.2022.3160482>
9. **Sani, M.H., Khosroabadi, S.** A Novel Design and Analysis of High-Sensitivity Biosensor Based on Nano-Cavity for Detection of Blood Component, Diabetes, Cancer and Glucose Concentration *IEEE Sensors Journal* 20 (13) 2020: pp. 7161–7168.  
<https://doi.org/10.1109/JSEN.2020.2964114>
10. **Hu, S., Shi, Z., Zheng, R., Ye, W., Gao, X., Zhao, W., Yang, G.** Superhydrophobic Liquid-Solid Contact Triboelectric Nanogenerator as a Droplet Sensor for Biomedical Applications *ACS Applied Materials & Interfaces* 12 (36) 2020: pp. 40021–40030.  
<https://doi.org/10.1021/acsami.0c10097>
11. **Güneş, İ.L., Oktay, B.** Fabrication of Eco-Friendly Sustainable Superhydrophobic and Anticorrosive Coatings from Acrylated Soybean Oil and Biobased Amine by the Aza-Michael Reaction *ACS Sustainable Chemistry & Engineering* 11 (42) 2023: pp. 15253–15261.  
<https://doi.org/10.1021/acssuschemeng.3c03169>
12. **Sun, H., Li, T., Lei, F., Lyu, S., Yang, Y., Li, B., Han, H., Wu, B., Huang, J., Zhang, C.** Fast Self-Healing Superhydrophobic Thermal Energy Storage Coatings Fabricated by Bio-Based Beeswax and Artificially Cultivated Diatom Frustules *ACS Applied Materials & Interfaces* 13 (40) 2021: pp. 48088–48100.  
<https://doi.org/10.1021/acsami.1c14065>
13. **Peng, J., Wu, L., Zhang, H., Wang, B., Si, Y., Jin, S., Zhu, H.** Research Progress on Eco-Friendly Superhydrophobic Materials in Environment, Energy and Biology *Chemical Communications* 58 (80) 2022: pp. 11201–11219.  
<https://doi.org/10.1039/D1NA00296A>

14. **Olson, E., Blisko, J., Du, C., Liu, Y., Li, Y., Thurber, H., Curtzwiler, G., Ren, J., Thuo, M., Yong, X.** Biobased Superhydrophobic Coating Enabled by Nanoparticle Assembly *Nanoscale Advances* 3 (14) 2021: pp. 4037–4047.  
<https://doi.org/10.1039/D1NA00296A>
15. **Shen, Y., Wu, Z., Tao, J., Jia, Z., Chen, H., Liu, S., Jiang, J., Wang, Z.** Spraying Preparation of Eco-Friendly Superhydrophobic Coatings with Ultralow Water Adhesion for Effective Anticorrosion and Antipollution *ACS Applied Materials & Interfaces* 12 (22) 2020: pp. 25484–25493.  
<https://doi.org/10.1021/acsmami.0c06074>
16. **Ghosh, P., Biswas, S., Kushagra, A.** Development of Conductometric Glucose Sensor in Nanomolar (Nm) Range from Phantom Blood Serum *Materials Today: Proceedings* 80 2023: pp. 1865–1867.  
<https://doi.org/10.1016/j.matpr.2021.05.627>
17. **Teymourian, H., Barfidokht, A., Wang, J.** Electrochemical Glucose Sensors in Diabetes Management: An Updated Review (2010–2020) *Chemical Society Reviews* 49 (21) 2020: pp. 7671–7709.  
<https://doi.org/10.1039/D0CS00304B>
18. **Tang, X., Huang, W., Xie, Y., Xiao, Z., Wang, H., Liang, D., Li, J., Wang, Y.** Superhydrophobic Hierarchical Structures from Self-Assembly of Cellulose-Based Nanoparticles *ACS Sustainable Chemistry & Engineering* 9 (42) 2021: pp. 14101–14111.  
<https://doi.org/10.1021/acssuschemeng.1c03876>
19. **Ganewatta, M.S., Wang, Z., Tang, C.** Chemical Syntheses of Bioinspired and Biomimetic Polymers toward Biobased Materials *Nature Reviews Chemistry* 5 (11) 2021: pp. 753–772.  
<https://doi.org/10.1038/s41570-021-00325-x>
20. **Abdolrazzagli, M., Katchinskiy, N., Elezzabi, A.Y., Light, P.E., Daneshmand, M.** Noninvasive Glucose Sensing in Aqueous Solutions Using an Active Split-Ring Resonator *IEEE Sensors Journal* 21 (17) 2021: pp. 18742–18755.  
<https://doi.org/10.1109/JSEN.2021.3090050>



© Lan et al. 2026 Open Access This article is distributed under the terms of the Creative Commons Attribution 4.0 International License (<http://creativecommons.org/licenses/by/4.0/>), which permits unrestricted use, distribution, and reproduction in any medium, provided you give appropriate credit to the original author(s) and the source, provide a link to the Creative Commons license, and indicate if changes were made.